# Data Complexity-Oriented Classification of Multispectral Remote Sensing Imagery via Machine and Deep Learning Approaches

Berrin Islek[1][a] and Hamza Erol[2][b]
[1]Department of Computer Engineering, Sivas Science and Technology University, Sivas, Turkey
[2]Department of Computer Engineering, Mersin University, Mersin, Turkey

Keywords: Deep Neural Network, Data Complexity, Computational Complexity, Information Complexity, Support Vector Machines, Random Forest.

Abstract: In this study, the land cover of an agricultural region was classified at a field level using multispectral satellite imagery. The primary objective of the study was to evaluate different classification methods in terms of data complexity, computational complexity, and information complexity. The data labelling process was performed using hierarchical clustering, making the groups in the data more meaningful. A separate clustering tree structure was created for each feature, and data complexity was analysed using parameters such as level, number of families, and number of children. Object-oriented approaches were adopted in the classification phase, employing Deep Neural Networks, Random Forest, and Support Vector Machines. The performance of these methods was examined not only in terms of accuracy but also in terms of evaluation metrics such as F1-score, recall, and precision. The results demonstrate the classification capabilities of the methods in a comprehensive manner and provide important clues about which approach is more suitable in different scenarios. Furthermore, the methods were compared in terms of computational costs and processing times, and a comprehensive evaluation was conducted regarding the classification of agricultural regions using remotely sensed data.



## 1 INTRODUCTION

Multispectral remote sensing images are widely used to classify vegetation types and estimate crop yields in agricultural regions (Thyagharajan and Vignesh, 2019; Modica et al., 2021). This approach has emerged as a key resource in contemporary precision agriculture, allowing extensive assessment of crop conditions, vegetation patterns, and soil characteristics (Sishodia et al., 2020; Guanter et al., 2013). These images capture data across multiple spectral bands, providing information that is not visible to the human eye, which is crucial for accurate assessment of crop status and yield prediction (Thenkabail, Lyon, & Huete, 2016).

Over the years, various approaches have been proposed to improve classification accuracy using multispectral images. For example, Erol and Akdeniz employed mixture distribution models for land cover classification, achieving an accuracy of 94% (Erol & Akdeniz, 2005). Sehgal applied preprocessing techniques and different classification algorithms to multispectral satellite images, reaching a maximum accuracy of 87% using a Backpropagation Neural Network (BPNN) (Sehgal, 2012). Similarly, Çalış and Erol (2012) applied mixture discriminant analysis, while Crnojević et al. (2014) integrated Landsat-8 and RapidEye images for pixel-based classification in northern Serbia. Gogebakan and Erol (2018) developed a semi-supervised approach for classifying multispectral data, which utilizes clustering based on mixture models. Sicre et al. (2020) analyzed the contribution of microwave and optical data for land type classification in southwestern France, achieving up to 85% accuracy using Support Vector Machines and Random Forests.

Selecting an appropriate classification method for multispectral satellite imagery of agricultural regions containing diverse crop types remains a critical task. To address this challenge, numerous machine

[a] https://orcid.org/ 0000-0003-1984-357X
[b] https://orcid.org/0000-0001-8983-4797



Islek, B. and Erol, H.
Data Complexity-Oriented Classification of Multispectral Remote Sensing Imagery via Machine and Deep Learning Approaches.
DOI: 10.5220/0014313500004848

In *Proceedings of the 2nd International Conference on Advances in Electrical, Electronics, Energy, and Computer Sciences (ICEEECS 2025)*, pages 257-265
ISBN: 978-989-758-783-2

learning and deep learning algorithms have been developed to improve land use and vegetation classification accuracy. In Dash et al. (2023) study, LandSat image data was used to increase the accuracy of land use and vegetation classification in agricultural regions. In this study, Support Vector Machines (SVM) (Kadavi & Lee, 2018; Singh, Gayathri, & Chaudhuri, 2022), Random Forest Classifier (RFC) (Pal, 2005; Zhang et al., 2017), and Deep Neural Networks (DNN) (Singh et al., 2025) were used. The objectives of this study are as follows: First, the complexity of remotely sensed multi-spectral satellite imagery will be calculated and data labeling will be performed. Then, we will classify remotely sensed multi-spectral satellite imagery of agricultural regions using object-based SVM, RFC, and DNN classification methods and compare the classification performance of these three methods. Finally, the obtained results will be evaluated and discussed.

## 2 MATERIALS AND METHOD

In this section, we provide a comprehensive description of the study workflow. Specifically, we discuss (i) the remotely sensed multispectral images of the agricultural region under study, (ii) the complexity of these data, (iii) the data labelling process, (iv) the classification methods applied to these datasets, and (v) the performance evaluation metrics used to assess the models.

### 2.1 Remotely Sensed Multispectral Image of Agricultural Region

The multispectral imagery employed in this research was obtained using the Landsat Thematic Mapper and depicts an agricultural region situated in the Seyhan Plain (approximately 37° N, 36° E) in Adana, Turkey. The image spans an area of 198 × 200 pixels, resulting in a total of 39,600 pixels, and was acquired on 27 March 1992 (Path 175–Row 34). For analysis, bands 3, 4, and 5 were selected, as they are effective in differentiating healthy vegetation, open water, and soil surfaces, respectively. Figure 1 presents the Landsat Thematic Mapper image of the study area without incorporating prior field information.

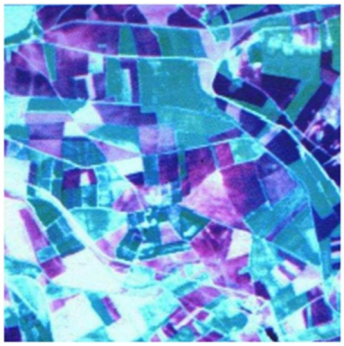

Figure 1: Landsat Thematic Mapper image, without a prior information, of the agricultural region studied.

The study area consists of 269 individual fields, labeled with codes from F001 to F269 on the parcelization map prepared by the Government Irrigation Department (DSI). Five major land cover classes—wheat, potato, vegetable garden, citrus, and bare soil—are present in the region, with a total of 24 subcategories. Based on this classification, 24 control fields have been defined within the area.

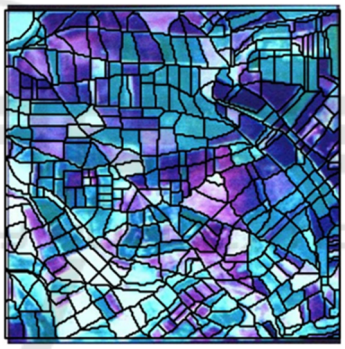

Figure 2: Landsat Thematic Mapper image of the study area, incorporating the previously collected parcel information.

Based on a land cover survey, the control plots were designated with identifiers CF001 to CF024 on the parcel map provided by the Government Irrigation Department. The remaining 245 plots, serving as test sites, were labeled TF001 through TF245 on the same map. Figure 2 shows a Landsat Thematic Mapper image of the study area, incorporating the previously collected parcel information.

### 2.2 Data Complexity Analysis of Multispectral Remote Sensing Image in Agricultural Regions

The multispectral image data analysed in this study were acquired using the Landsat Thematic Mapper sensor. Let's bands 3, 4 and 5 values denoted by

variables $X_1$, $X_2$ and $X_3$ respectively. There are 39600 instances (observations) surrounding 198x200 data matrix for each variable (feature).

The method for determining the degree of data complexity is based on hierarchical structure of all groups and all clusters in data (Erol & Erol, 2018). The assessment of data complexity is conducted by utilizing the hierarchical tree structure of groups and clusters based on the features of the data. The tree structures are obtained by finding all groups for each feature in data. The hierarchical tree structures of all groups in each feature for obtaining remotely sensed multispectral image data complexity were shown in Fig. 3 – Fig. 5 respectively.

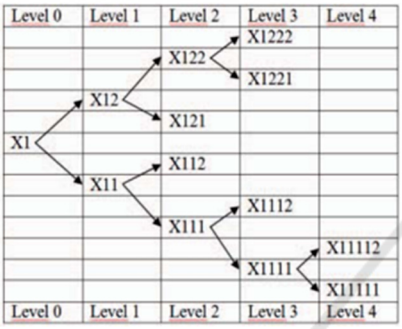


Figure 3: The hierarchical tree structures of all groups in the first feature $X_1$ for remotely sensed multispectral image data complexity.

The number of levels is 4, the number of parent nodes ($npn_1$) is 5 and the number of child nodes ($ncn_1$) is 7 in hierarchical tree structures of all groups in feature $X_1$ for remotely sensed multispectral image data as shown in Fig 3 (Erol & Erol, 2018).

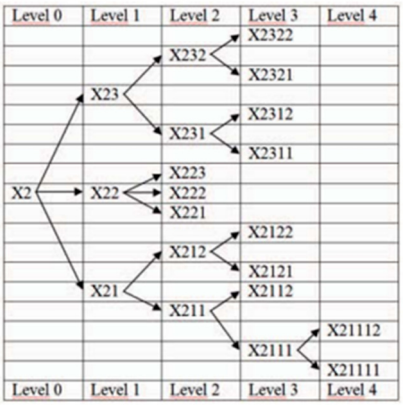


Figure 4: The hierarchical tree structures of all groups in the second feature $X_2$ for remotely sensed multispectral image data complexity.

The number of levels is 4, the number of parent nodes ($npn_2$) is 8 and the number of child nodes ($ncn_2$) is 12 in hierarchical tree structures of all groups in feature $X_2$ for remotely sensed multispectral image data as shown in Fig 4 (Erol & Erol, 2018).

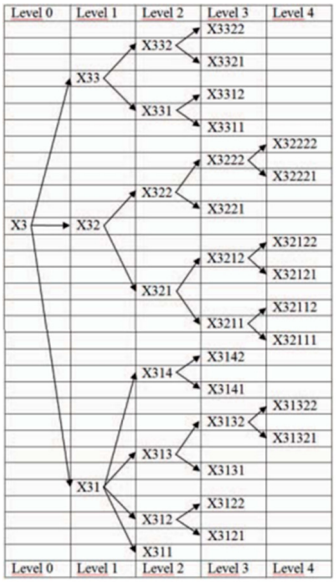


Figure 5: The hierarchical tree structures of all groups in the third feature $X_3$ for remotely sensed multispectral image data complexity.

The number of levels is 4, the number of parent nodes ($npn_3$) is 14 and the number of child nodes ($ncn_3$) is 19 in hierarchical tree structures of all groups in feature $X_3$ for remotely sensed multispectral image data as shown in Fig 5 [18].

Let $ncn_i$ and $npn_i$ denote the number of child nodes and parent nodes for feature $X_i$ respectively. Let $DCX_i$ denote data complexity for feature $X_i$. Then the data complexity for each feature $X_i$ is defined as

$$DCX_i = ncn_i - npn_i \quad \text{for } i=1,2,3 \tag{1}$$

So $DCX_1 = 2$, $DCX_2 = 4$ and $DCX_3 = 5$ for i=1,2,3 respectively. Let DC denote the data complexity for entire data. Thus for all features. Then DC is defined as:

$$DC = \prod_{i=1}^{3} DCX_i \tag{2}$$

$DCX_1 = 2$, $DCX_2 = 4$ and $DCX_3 = 5$ for feature $X_1$, $X_2$ and $X_3$ are 2, 4 and 5 respectively. Then the data complexity for entire data $DC = DCX_1 * DCX_2 * DCX_3 = 2 * 4 * 5 = 40$. In the rest of this study, with this DC = 40 for entire data which classification method among three methods give the best classification performance will be determined. Thus, which method? Machine learning methods versus deep learning method.

## 2.3 Data Labelling of Remotely Acquired Images for Agricultural Lands

Two types of data are considered in this study: incomplete data, which lack class labels, and complete data, which include class labels. Class labels (or class codes) are essential for the classification of vector data. For the remotely sensed multispectral image data of the agricultural area, data labelling was performed based on the field (parcel) structure within the region. A total of 245 test fields and 24 control fields were identified in the multispectral imagery using an edge detection algorithm in conjunction with the parcelization map of the agricultural area. The field types and corresponding class codes are listed in Table 1.

Table 1: Control field codes and data labels (class codes).

| Field Types | Data Labels |
|---|---|
| Wheat1 | 1 |
| Wheat2 | 2 |
| Wheat3 | 3 |
| Wheat4 | 4 |
| Wheat5 | 5 |
| Wheat6 | 6 |
| Potato1 | 7 |
| Potato2 | 8 |
| Potato3 | 9 |
| Potato4 | 10 |
| Vegetable garden1 | 11 |
| Vegetable garden2 | 12 |
| Vegetable garden3 | 13 |
| Vegetable garden4 | 14 |
| Vegetable garden5 | 15 |
| Vegetable garden6 | 16 |
| Citrus1 | 17 |
| Citrus2 | 18 |
| Citrus3 | 19 |
| Citrus4 | 20 |
| Bare soil1 | 21 |
| Bare soil2 | 22 |
| Bare soil3 | 23 |
| Bare soil4 | 24 |
| Bare soil5 | 25 |

Data labelling is made for totally 39600 instances (observations) in the 245 test fields and 24 control fields of remotely sensed multispectral image data in the agricultural area. Complete data is obtained as comma separated values data file.

## 2.4 Classification Methods

The Support Vector Machine (SVM) is a supervised learning algorithm grounded in Vapnik's statistical learning theory (Vapnik, 2013). Its main objective is to identify the optimal separation boundaries between classes. By using a kernel function, SVM can project training examples into a higher-dimensional space, allowing it to distinguish classes that are not linearly separable in the original feature space. The selection of the kernel function is a key design choice. Typical kernels include linear, polynomial, radial basis function (RBF), and sigmoid. In this study, the RBF kernel is chosen because of its effectiveness in managing non-linear separation tasks (Kadavi & Lee, 2018).

The Random Forest Classifier (RFC) is an ensemble learning technique that generates a collection of decision trees, each trained on randomly selected subsets of data and features. At every split within a tree, only a randomly chosen portion of the available attributes is considered for determining the division (Breiman, 1999). Each tree produces its own prediction for a given input, and the final classification outcome is obtained through majority voting across the ensemble. This approach improves model stability and helps mitigate overfitting. For the induction of individual decision trees, a feature selection criterion and a pruning strategy must be specified. Among the available criteria, the Gini index is widely used to select the most informative feature at each split. The aggregation of predictions from the N randomly constructed trees forms the foundation of the Random Forest algorithm. Subsequently, the trained forest is used to predict the labels of samples in the test dataset, and the class with the most votes across the trees is assigned as the final prediction (Pal, 2005).

A Deep Neural Network (DNN) is an advanced type of artificial neural network designed to capture complex relationships in data through multiple layers of interconnected neurons. Inspired by the information processing mechanisms of the human brain, DNNs consist of several hidden layers, where each layer transforms the output of the previous layer into increasingly abstract representations. Training typically involves the backpropagation algorithm, which adjusts network weights by propagating prediction errors backward, allowing the network to improve its performance iteratively. The effectiveness of a DNN depends on several factors, including structural choices such as the number of layers and neurons per layer, learning parameters such as activation functions, learning rate, number of

epochs, batch size, and the use of regularization methods. These factors collectively influence how well the network learns patterns, generalizes unseen data, and avoids overfitting. DNNs are particularly suitable for handling large-scale and high-dimensional datasets due to their capacity for hierarchical feature extraction (Schmidhuber, 2014).

## 2.5 Performance Measures

Evaluating classification models requires not only the correct implementation of algorithms but also the selection of appropriate performance metrics. These metrics quantify how well a model predicts class labels and help identify which aspects of performance are most relevant for a given application. For balanced datasets, accuracy may provide a sufficient measure, whereas for imbalanced datasets, precision, recall, and F1-score offer more informative assessments. Therefore, multiple metrics are typically reported rather than relying on a single measure.

In classification tasks, the performance of a model is commonly evaluated by comparing its predicted labels with the actual labels. These results can be summarized in a confusion matrix, which presents the counts of correctly and incorrectly classified samples. Instances that are correctly predicted as positive are referred to as True Positives (TP), whereas correctly predicted negative instances are True Negatives (TN). False Positives (FP) indicate negative cases that were mistakenly classified as positive, and False Negatives (FN) represent positive cases incorrectly identified as negative. These counts serve as the basis for computing various performance metrics.

Accuracy, for example, quantifies the ratio of correctly classified samples to the total number of observations. (see Eq. 3)

$$Accuracy = \frac{\mathrm{TP+TN}}{\mathrm{TP+TN+FP+FN}} \tag{3}$$

Precision indicates the fraction of predicted positive instances that are actually positive, reflecting the model's reliability in its positive predictions. (see Eq. 4)

$$Precision = \frac{\mathrm{TP}}{\mathrm{TP+FP}} \tag{4}$$

Recall, also referred to as sensitivity, measures the fraction of actual positive instances that the model successfully identifies, capturing its ability to detect positive cases. (see Eq. 5)

$$Recall = \frac{\mathrm{TP}}{\mathrm{TP+FN}} \tag{5}$$

The F1-score provides a balanced assessment by combining precision and recall through their harmonic mean, offering a single measure that considers both false positives and false negatives. (see Eq. 6) (Dalianis, 2018)

$$F1\ score = 2 * \frac{\mathrm{Precision*Recall}}{\mathrm{Precision+Recall}} \tag{6}$$

These metrics together offer a comprehensive evaluation of classification performance and were used to assess the predictive models in this study.

# 3 RESULTS

In this section, all classification experiments were conducted using Python and executed on the high-performance computing environment provided by Google Colab (Google Research, 2025). For each model, classification reports were generated to evaluate class-wise performance metrics such as accuracy, precision, recall, and F1-score. In addition, confusion matrices were analyzed to better understand misclassification patterns between different classes. The following subsections present the results obtained for each classification method applied to the multispectral remote sensing dataset.

## 3.1 SVM-Based Classification Outcomes of Remotely Sensed Multispectral Data

The first classification experiment was conducted using the Support Vector Machine (SVM) algorithm. The multispectral remote sensing dataset was divided into training (80%) and testing (20%) subsets. Class-based evaluation metrics such as precision, recall, and F1-score are presented in Table 2, while the corresponding confusion matrix is illustrated in Fig 6. These results provide insights into the SVM model's ability to accurately distinguish between the different land cover classes.

The SVM model achieved an overall accuracy of 95%, with weighted average precision, recall, and F1-score also around 95%, indicating a generally balanced performance across the dataset. While the model performed well for most classes, some underrepresented classes showed lower recall values, reflecting occasional misclassifications. Very small classes exhibited extreme metric values, with some appearing perfect due to overfitting rather than genuine predictive capability. The confusion matrix (Fig.6) highlights the distribution of misclassifications

and provides insight into the model's strengths and weaknesses.

Table 2: Classification report for the SVM model applied to the image data used in the study.

| Class | Precision | Recall | F1-score | Support |
|---|---|---|---|---|
| 1 | 0.95 | 0.97 | 0.96 | 492 |
| 2 | 0.93 | 0.99 | 0.96 | 235 |
| 3 | 0.99 | 0.96 | 0.97 | 359 |
| 4 | 1.00 | 0.47 | 0.64 | 19 |
| 5 | 0.93 | 0.94 | 0.94 | 378 |
| 6 | 0.94 | 0.84 | 0.89 | 133 |
| 7 | 0.95 | 0.95 | 0.95 | 188 |
| 8 | 0.92 | 0.90 | 0.91 | 226 |
| 9 | 0.98 | 0.93 | 0.96 | 283 |
| 10 | 0.95 | 0.99 | 0.97 | 1194 |
| 11 | 0.91 | 0.96 | 0.94 | 371 |
| 12 | 0.91 | 0.93 | 0.92 | 122 |
| 13 | 0.95 | 0.99 | 0.97 | 562 |
| 14 | 0.99 | 0.93 | 0.96 | 568 |
| 15 | 0.85 | 0.64 | 0.73 | 36 |
| 16 | 1.00 | 0.74 | 0.85 | 19 |
| 17 | 0.95 | 0.97 | 0.96 | 512 |
| 18 | 0.91 | 0.86 | 0.88 | 143 |
| 19 | 0.98 | 0.96 | 0.97 | 379 |
| 20 | 0.00 | 0.00 | 0.00 | 2 |
| 21 | 0.97 | 0.94 | 0.95 | 262 |
| 22 | 0.97 | 0.95 | 0.96 | 297 |
| 23 | 1.00 | 1.00 | 1.00 | 4 |
| 24 | 0.97 | 0.96 | 0.96 | 837 |
| 25 | 0.93 | 0.94 | 0.94 | 299 |
| Accuracy | | | 0.95 | 7920 |
| Macro Avg | 0.91 | 0.87 | 0.89 | 7920 |
| Weighted Avg | 0.95 | 0.95 | 0.95 | 7920 |

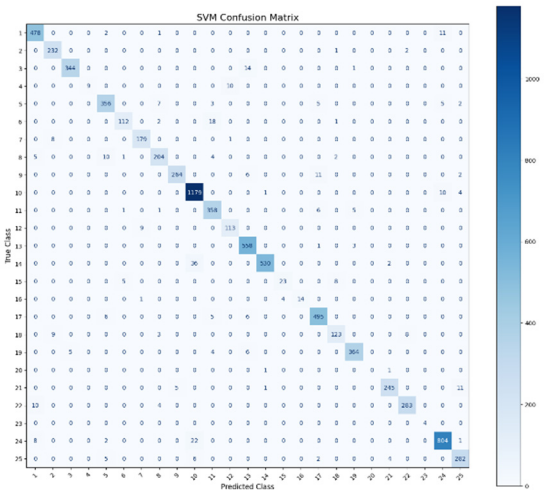


Figure 6: Confusion matrix of the image data used in the study using SVM.

## 3.2 RFC-Based Classification Outcomes of Remotely Sensed Multispectral Data

In Next, the Random Forest (RF) method was applied to the dataset to evaluate its classification performance. The multispectral remote sensing dataset was divided into training (80%) and testing (20%) subsets. Class-wise metrics are summarized in Table 3, and the corresponding confusion matrix is shown in Figure 7. The results illustrate the RF algorithm's handling of class separability and highlight its comparative strengths and limitations.

Table 3: Classification report for the RFC model applied to the image data used in the study.

| Class | Precision | Recall | F1-score | Support |
|---|---|---|---|---|
| 1 | 0.99 | 1.00 | 0.99 | 492 |
| 2 | 0.95 | 0.97 | 0.96 | 235 |
| 3 | 1.00 | 0.99 | 0.99 | 359 |
| 4 | 1.00 | 0.84 | 0.91 | 19 |
| 5 | 0.94 | 0.95 | 0.94 | 378 |
| 6 | 0.94 | 0.98 | 0.96 | 133 |
| 7 | 0.97 | 0.96 | 0.97 | 188 |
| 8 | 0.93 | 0.93 | 0.93 | 226 |
| 9 | 0.99 | 0.98 | 0.98 | 283 |
| 10 | 0.99 | 1.00 | 0.99 | 1194 |
| 11 | 0.96 | 0.97 | 0.97 | 371 |
| 12 | 0.98 | 0.98 | 0.98 | 122 |
| 13 | 0.99 | 1.00 | 0.99 | 562 |
| 14 | 0.99 | 1.00 | 0.99 | 568 |
| 15 | 0.91 | 0.86 | 0.89 | 36 |
| 16 | 1.00 | 0.79 | 0.88 | 19 |
| 17 | 0.96 | 0.96 | 0.96 | 512 |
| 18 | 0.92 | 0.92 | 0.92 | 143 |
| 19 | 0.98 | 0.98 | 0.98 | 379 |
| 20 | 0.00 | 0.00 | 0.00 | 2 |
| 21 | 1.00 | 0.99 | 0.99 | 262 |
| 22 | 0.97 | 0.96 | 0.97 | 297 |
| 23 | 1.00 | 1.00 | 1.00 | 4 |
| 24 | 1.00 | 0.99 | 0.99 | 837 |
| 25 | 0.96 | 0.97 | 0.97 | 299 |
| Accuracy | | | 0.98 | 7920 |
| Macro Avg | 0.93 | 0.92 | 0.92 | 7920 |
| Weighted Avg | 0.98 | 0.98 | 0.98 | 7920 |

The Random Forest model achieved an overall accuracy of 98%, with weighted average precision, recall, and F1-score also at 98%, demonstrating strong and consistent performance across the dataset. Although the model performed exceptionally well overall, lower recall values were observed for some

underrepresented classes, indicating occasional misclassifications. Very small classes again showed extreme metric values, which may be indicative of overfitting. The confusion matrix (Fig.7) illustrates the patterns of misclassification and highlights the model's general strengths and limitations.

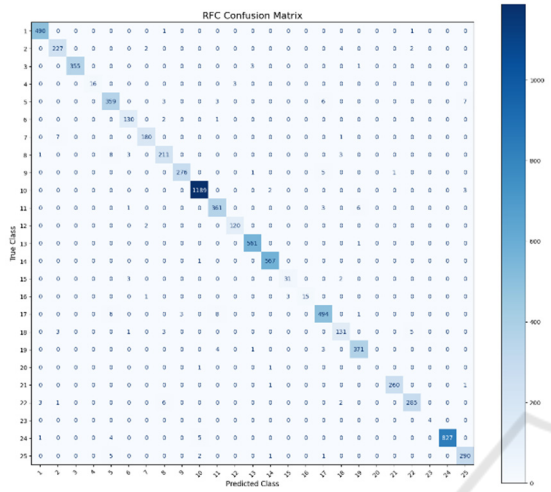


Figure 7: Confusion matrix of the image data used in the study using RFC.

## 3.3 DNN-Based Classification Outcomes of Remotely Sensed Multispectral Data

Finally, a Deep Neural Network (DNN) model was trained and tested to assess the effectiveness of a deep learning-based approach. The multispectral remote sensing dataset was divided into training (80%) and testing (20%) subsets. Evaluation metrics for each class are presented in Table 4, while the confusion matrix is provided in Figure 8. These results demonstrate the DNN model's capability to capture complex patterns in the multispectral data and serve as a benchmark for comparing machine learning and deep learning approaches.

The DNN model achieved an overall accuracy of 97%, with weighted average precision, recall, and F1-score also at 97%, indicating a strong and balanced performance across the dataset. While the model performed well for most classes, some underrepresented classes exhibited lower recall values, reflecting occasional misclassifications. Very small classes showed extreme metric values in some cases, which may indicate overfitting rather than genuine predictive performance. The confusion matrix (Figure 8) illustrates the distribution of misclassifications and highlights the general strengths and limitations of the model.

Table 4: Classification report for the DNN model applied to the image data used in the study.

| Class | Precision | Recall | F1-score | Support |
|---|---|---|---|---|
| 1 | 0.99 | 0.95 | 0.97 | 492 |
| 2 | 0.96 | 0.99 | 0.97 | 235 |
| 3 | 0.90 | 1.00 | 0.95 | 359 |
| 4 | 0.86 | 1.00 | 0.93 | 19 |
| 5 | 0.99 | 0.94 | 0.96 | 378 |
| 6 | 0.95 | 0.98 | 0.96 | 133 |
| 7 | 0.94 | 0.99 | 0.97 | 188 |
| 8 | 0.91 | 0.97 | 0.94 | 226 |
| 9 | 0.95 | 0.99 | 0.97 | 283 |
| 10 | 0.98 | 0.99 | 0.99 | 1194 |
| 11 | 0.97 | 0.98 | 0.97 | 371 |
| 12 | 0.99 | 0.93 | 0.93 | 122 |
| 13 | 0.98 | 0.94 | 0.96 | 562 |
| 14 | 0.98 | 0.99 | 0.99 | 568 |
| 15 | 1.00 | 0.75 | 0.86 | 36 |
| 16 | 0.82 | 0.95 | 0.88 | 19 |
| 17 | 0.99 | 0.94 | 0.96 | 512 |
| 18 | 0.91 | 0.96 | 0.94 | 143 |
| 19 | 0.98 | 0.98 | 0.86 | 379 |
| 20 | 0.67 | 1.00 | 0.98 | 2 |
| 21 | 1.00 | 0.96 | 0.98 | 262 |
| 22 | 0.94 | 0.98 | 0.96 | 297 |
| 23 | 1.00 | 1.00 | 1.00 | 4 |
| 24 | 1.00 | 0.98 | 0.99 | 837 |
| 25 | 0.99 | 0.97 | 0.98 | 299 |
| Accuracy | | | 0.97 | 7920 |
| Macro Avg | 0.95 | 0.96 | 0.95 | 7920 |
| Weighted Avg | 0.97 | 0.97 | 0.97 | 7920 |

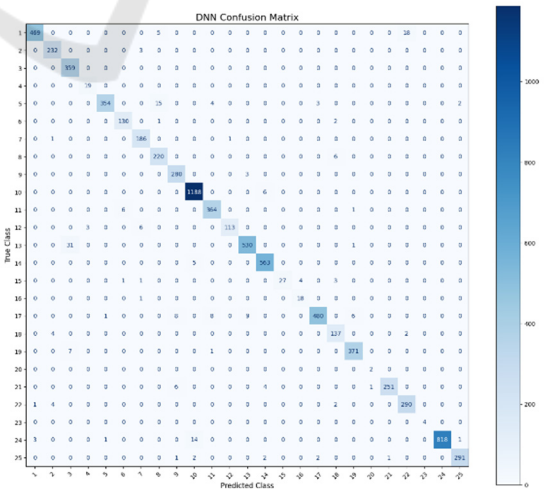


Figure 8: Confusion matrix of the image data used in the study using DNN.

# 4 DISCUSSION AND CONCLUSION

Classification reports are presented in Tables 2, 3, and 4, respectively, and confusion matrices are presented in Figs. 6, 7, and 8, respectively, obtained from the three classification methods: SVM, RFC, and DNN. Accuracy, precision, recall, and f1 score are calculated from the confusion matrix results.

The overall accuracies of the SVM, RFC, and DNN are 0.96, 0.99, and 0.95 in Table 2, Table 3, and Table 4, respectively. As explained in Section 2, the best classification accuracy result calculated from the DNNs is 0.95 due to data complexity. Based on the results in the precision and/or recall columns, the f1-score columns of SVM and RFC cannot distinguish or classify some classes, as can be seen in Tables 2 and 3. However, based on the results in the precision and recall columns, the f1-score column of DNN can distinguish or classify all classes, as can be seen in Table 4. Due to the greater number of processing layer steps, the processing time is the longest for DNN.

The findings of this study indicate that when the data complexity is low, classification can be effectively performed using machine learning techniques, whereas high data complexity may require the utilization of deep learning approaches.

# REFERENCES


Thyagharajan, K. K., & Vignesh, T. (2019). Soft computing techniques for land use and land cover monitoring with multispectral remote sensing images: A review. *Archives of Computational Methods in Engineering*, *26*(2), 275-301.

Modica, G., De Luca, G., Messina, G., & Praticò, S. (2021). Comparison and assessment of different object-based classifications using machine learning algorithms and UAVs multispectral imagery: A case study in a citrus orchard and an onion crop. *European Journal of Remote Sensing*, *54*(1), 431-460.

Sishodia, R. P., Ray, R. L., & Singh, S. K. (2020). Applications of remote sensing in precision agriculture: A review. *Remote sensing*, *12*(19), 3136.

Guanter, L., Rossini, M., Colombo, R., Meroni, M., Frankenberg, C., Lee, J. E., & Joiner, J. (2013). Using field spectroscopy to assess the potential of statistical approaches for the retrieval of sun-induced chlorophyll fluorescence from ground and space. *Remote Sensing of Environment*, *133*, 52-61.

Thenkabail, P. S., Lyon, J. G., & Huete, A. (2016). Hyperspectral remote sensing of agriculture and vegetation. *Remote Sensing of Environment, 185,* 1–17. https://doi.org/10.1016/j.rse.2016.01.005

Erol, H., & Akdeniz, F. (2005). A per-field classification method based on mixture distribution models and an application to Landsat Thematic Mapper data. *International Journal of Remote Sensing, 26*(6), 1229–1244. https://doi.org/10.1080/01431160512331326800

Sehgal, S. (2012). Remotely sensed LANDSAT image classification using neural network approaches. *International Journal of Engineering Research and Applications, 2*(5), 43–46.

Calış, N., & Erol, H. (2012). A new per-field classification method using mixture discriminant analysis. *Journal of Applied Statistics, 39*(10), 2129–2140. https://doi.org/10.1080/02664763.2012.702263

Crnojević, V., Lugonja, P., Brkljač, B., & Brunet, B. (2014). Classification of small agricultural fields using combined Landsat-8 and RapidEye imagery: Case study of northern Serbia. *Journal of Applied Remote Sensing, 8*(1), 083512. https://doi.org/10.1117/1.JRS.8.083512

Gogebakan, M., & Erol, H. (2018). A new semi-supervised classification method based on mixture model clustering for classification of multispectral data. *Journal of the Indian Society of Remote Sensing, 46*(8), 1323–1331. https://doi.org/10.1007/s12524-018-0808-9

Sicre, C. M., Fieuzal, R., & Baup, F. (2020). Contribution of multispectral (optical and radar) satellite images to the classification of agricultural surfaces. *International Journal of Applied Earth Observation and Geoinformation, 84,* 101972. https://doi.org/10.1016/j.jag.2019.101972

Dash, P., Sanders, S. L., Parajuli, P., & Ouyang, Y. (2023). Improving the accuracy of land use and land cover classification of Landsat data in an agricultural watershed. *Remote Sensing, 15*(16), 4020. https://doi.org/10.3390/rs15164020

Kadavi, P. R., & Lee, C. W. (2018). Land cover classification analysis of volcanic island in Aleutian Arc using an artificial neural network (ANN) and a support vector machine (SVM) from Landsat imagery. *Geosciences Journal, 22*(5), 653–665. https://doi.org/10.1007/s12303-018-0023-2

Singh, M. P., Gayathri, V., & Chaudhuri, D. (2022). A simple data preprocessing and postprocessing techniques for SVM classifier of remote sensing multispectral image classification. *IEEE Journal of Selected Topics in Applied Earth Observations and Remote Sensing, 15,* 1–10. https://doi.org/10.1109/JSTARS.2022.3201273

Pal, M. (2005). Random forest classifier for remote sensing classification. *International Journal of Remote Sensing, 26*(1), 217–222. https://doi.org/10.1080/01431160412331269698

Zhang, H., Li, Q., Liu, J., Shang, J., Du, X., McNairn, H., Champagne, C., Dong, T., & Liu, M. (2017). Image classification using RapidEye data: Integration of spectral and textual features in a random forest classifier. *IEEE Journal of Selected Topics in Applied Earth Observations and Remote Sensing, 10*(12), 1–10. https://doi.org/10.1109/JSTARS.2017.2774807

Singh, G., Vyas, N., Dahiya, N., Singh, S., Bhati, N., Sood, V., & Gupta, D. K. (2025). A novel pixel-based deep neural network in posterior probability space for the detection of agriculture changes using remote sensing data. *Remote Sensing Applications: Society and Environment, 38,* 101591. https://doi.org/10.1016/j.rsase.2025.101591

Erol, H., & Erol, R. (2018). Determining big data complexity using hierarchical structure of groups and clusters in decision tree. In *Proceedings of the 3rd International Conference on Computer Science and Engineering (UBMK'18)* (pp. 594–597). IEEE. https://doi.org/10.1109/UBMK.2018.8566398

Vapnik, V. (2013). *The nature of statistical learning theory.* Springer Science & Business Media.

Kadavi, P. R., & Lee, C. W. (2018). Land cover classification analysis of volcanic island in Aleutian Arc using an artificial neural network (ANN) and a support vector machine (SVM) from Landsat imagery. *Geosciences Journal, 22,* 653–665. https://doi.org/10.1007/s12303-018-0023-2

Breiman, L. (1999). Random forests—random features (Tech. Rep. No. 567). University of California, Berkeley, Department of Statistics.

Schmidhuber, J. (2014). Deep learning in neural networks: An overview. *Neural Networks, 61,* 85–117. https://doi.org/10.1016/j.neunet.2014.09.003

Dalianis, H. (2018). Evaluation metrics and evaluation. In *Clinical text mining: Secondary use of electronic patient records* (pp. 45–53). Springer.

Google Research. (2025). *Google Colab.* https://colab.research.google.com/